

Folded metaporous material for sub-wavelength and broadband perfect sound absorption

Cite as: Appl. Phys. Lett. **117**, 251902 (2020); <https://doi.org/10.1063/5.0032809>

Submitted: 11 October 2020 . Accepted: 08 December 2020 . Published Online: 24 December 2020

 Jean Boulvert,  Josué Costa-Baptista,  Théo Cavalieri,  Vicente Romero-García,  Gwénaél Gabard, Edith Roland Fotsing, Annie Ross, Maxime Perna, Jacky Mardjono, and  Jean-Philippe Groby



View Online



Export Citation



CrossMark

ARTICLES YOU MAY BE INTERESTED IN

[High thermal conductivity of free-standing skeleton in graphene foam](#)

Applied Physics Letters **117**, 251901 (2020); <https://doi.org/10.1063/5.0032408>

[A compact low-frequency sound-absorbing metasurface constructed by resonator with embedded spiral neck](#)

Applied Physics Letters **117**, 221902 (2020); <https://doi.org/10.1063/5.0031891>

[Direct current powered humidity sensor based on a polymer composite with humidity sensitive electronic conduction](#)

Applied Physics Letters **117**, 253303 (2020); <https://doi.org/10.1063/5.0030621>



Your Qubits. Measured.
Meet the next generation of quantum analyzers

- Readout for up to 64 qubits
- Operation at up to 8.5 GHz, mixer-calibration-free
- Signal optimization with minimal latency

[Find out more](#)



Folded metaporous material for sub-wavelength and broadband perfect sound absorption

Cite as: Appl. Phys. Lett. **117**, 251902 (2020); doi: [10.1063/5.0032809](https://doi.org/10.1063/5.0032809)

Submitted: 11 October 2020 · Accepted: 8 December 2020 ·

Published Online: 24 December 2020







View Online



Export Citation



CrossMark

Jean Boulvert,^{1,2,3,a)}  Josué Costa-Baptista,¹ Théo Cavalieri,^{2,3}  Vicente Romero-García,²  Gwénaél Gabard,²  Edith Roland Fotsing,¹ Annie Ross,¹ Maxime Perna,¹ Jacky Mardjono,³ and Jean-Philippe Groby² 

AFFILIATIONS

¹Laboratoire d'Analyse Vibratoire et Acoustique, LAVA, Mechanical engineering, Polytechnique Montréal, H3T 1J4 Montréal, Québec, Canada

²Laboratoire d'Acoustique de l'Université du Mans, LAUM-UMR CNRS 6613, Le Mans Université, Avenue Olivier Messiaen, 72085 Le Mans Cedex 9, France

³Safran Aircraft Engines, Rond Point René Ravaud-Réau, 77550 Moisy-Cramayel Cedex, France

^{a)} Author to whom correspondence should be addressed: jean.boulvert@univ-lemans.fr

ABSTRACT

This Letter reports a folded metaporous surface optimized to achieve sub-wavelength and broadband perfect absorption. Its unit cell is composed of four different helicoidal cavities filled by porous media, which are structured and quasi-isotropic micro-lattices with a variable lattice constant. The effective thickness and intrinsic losses of each helicoidal cavity can be adjusted independently by varying their macro- and micro-structures, namely, the number of revolution of the folded structure and the lattice constant of the micro-lattice. An analytical model predicting the physical properties of this metaporous surface is developed. The macro- and micro-structures are then jointly optimized for sub-wavelength broadband perfect absorption. Finally, the system is 3D printed and experimentally tested. The experimental results are found to be in good agreement with the theory and show an almost perfect absorption over a frequency range out of reach for the homogeneous constitutive porous medium and the only helicoidal cavities.

Published under license by AIP Publishing. <https://doi.org/10.1063/5.0032809>

In many practical applications, acoustic treatments are constrained to be thin to limit their associated bulk and mass. The downside is that it conflicts with the broadband absorption/attenuation of low- and medium-frequency noise. Indeed, the first resonance frequency f_0 of most acoustic treatments relying on Helmholtz (HR) or quarter-wavelength resonators (QWRs) such as liners is inversely related to their effective acoustic thickness L_a , i.e., the effective distance over which the pressure wave propagates. For example, f_0 of an L_a -thick straight QWR corresponds to a wavelength $\lambda = 4L_a$ when no losses are accounted for.

Open-cell porous layers form another class of widely used acoustic treatments. Their ability to operate as broadband acoustic absorbers is well established. However, their low- and medium-frequency efficiencies are limited by their thickness and their intrinsic loss mechanisms.¹ As the sound speed is smaller in porous materials than in air, the so-called “quarter-wavelength resonance” of such a layer is slightly shifted toward lower frequencies in comparison to that of an air-filled QWR and $\lambda \approx 5L_a$ is usually observed for a fibrous layer.² Open-cell porous materials can be 3D printed allowing the control of their

micro-structure and the tuning of their macroscopic properties.^{3–6} An efficient way to tackle the absorption of wavelengths many times larger than the thickness of the treatment consists in folding its constitutive elements.^{7–9} The equality between the effective acoustic thickness L_a and the bulk treatment thickness L_b is lifted and $L_a \geq L_b$, shifting down the corresponding resonance frequency while maintaining the treatment thickness. First, experimental and theoretical explorations were carried out on folded aeronautic liners.^{10,11} Models and geometries are still under development.^{7,8} More recently, the folding concept has been revisited to design notably acoustic metamaterial absorbers in the low-frequency range.⁹ Folding the geometry of the acoustic treatment elements helps in increasing the density of states at low frequencies. However, perfect absorption is required in addition to match the impedance of the acoustic treatment with that of the surrounding medium. The energy leakage of the acoustic treatment to the surrounding medium must be perfectly balanced by its inherent losses to satisfy this condition, also known as the critical coupling condition.¹² Recently, the concepts of folding and critical coupling have been combined to design sub-wavelength perfect absorbers,

based on folded QWR,¹³ HR,¹⁴ or other types of resonators.¹⁵ However, the absorption bandwidths of these kinds of perfect absorbers are narrow due to the high quality factor of their resonances. Therefore, combining a collection of detuned elements can lead to broadband perfect absorption.¹⁶

The concept of metaporous surface¹⁷ relies on the embedding of resonant elements^{18–21} to enhance the density of states at low frequency of a porous layer to achieve broadband and low-frequency absorption. The low-frequency absorption of the metaporous surface is higher than that of the single porous layer. The opposite approach, followed in this Letter, consists in using properly designed porous materials to enhance the absorption of folded metamaterials.

In this work, we theoretically and experimentally report folded resonators filled with 3D-printed open-cell porous materials, the resulting low quality factor resonances of which being critically coupled at normal incidence. Four different folded porous media (FPMs) working at different frequencies are designed and assembled in a metaporous surface (MpS) presenting a broadband quasi-perfect absorption at normal incidence for $5.6L_b < \lambda < 9.9L_b$. The MpS is mounted in a square waveguide of width $W = 41.9$ mm with a rigid backing and excited by a normal incident plane wave to mimic an infinite periodic acoustic treatment.²² This configuration is analytically modeled by the transfer matrix method inside the FPM coupled with a Bloch wave decomposition outside the MpS in order to account for the possible coupling between the FPM. This analytical model is used to calculate the reflection coefficient of the MpS. The MpS geometry is then optimized to maximize its absorption coefficient over a broadband frequency range by critically coupling each FPM. The optimized MpS is 3D printed and experimentally tested. Experimental results are in good agreement with both the analytical results and those obtained using Finite Element Method (FEM) numerical simulations.

A schematic of the MpS is shown in Fig. 1(a). It consists of four impervious folded helicoidal structures, inspired from Refs. 23 and 24, filled with different porous materials. The FPMs are labeled as shown in Figs. 1(a), 2(b), and 2(c), and their relative position is important. To create a FPM, a Greek cross of width $C/\sqrt{2}$ is run along the vertical (O, z_1) axis over a helix, generating a four branch helicoid. The latter is then encapsulated in a square cuboid of height L_b and width $C = W/2$ [see Fig. 1(b)]. Other folding strategies could be applied. The main advantage of this strategy is that the folding of each FPM can be done independent of that of the other FPMs: the FPMs are not

tangled together. The number of revolutions operated by the helix over the height L_b is denoted as ζ . The generated helicoidal cavities are then filled with a homogeneous anisotropic porous material as depicted in Fig. 1(d), creating the FPM. The pressure waves propagate along an helical mean path depicted by the gold arrows in Fig. 1(b) with a length $L_a \geq L_b$.

The considered filling porous material is the micro-lattice (ML) depicted in Fig. 1(f) composed of a superposition of parallel fibers orthogonally alternating in the (O, y_1, z_1) plane. Each fiber is a combination of two filaments of diameter $D = 200 \mu\text{m}$ merged with one another in the (O, z_1) direction. The distance between two micro-layers in the (O, z_1) direction is $0.9D$ to guarantee the bonding between filaments. Then, the representative unit cell consists of the junction of two orthogonal fibers as highlighted in Fig. 1(f). It is described by two micro-structural parameters: the filament diameter D and the spacing between two adjacent fibers in the (O, x_1, y_1) plane, i.e., the lattice constant AD , where $A > 1$. The pore size is defined here as the minimum distance between two adjacent fibers. In the z_1 direction, the pores are square and the pore size is equal to $H = D(A - 1)$. In the x_1 and y_1 directions, the pores are rectangular and of size $H \times 1.8D$. Thus, the medium is structured, periodic, and quasi-isotropic. The manufacturing variable that regulates the lattice constant is the “infill factor” IF , which can only take integer percent values. The relation between the infill factor IF and lattice constant is simply $IF(\%) = 100/A$.

The FPMs are made by the Fused Deposition Modeling (FDM) additive manufacturing technique: the printer successively adds micro-layers made of extruded filaments on top of each other. The extruded material is polylactic acid (PLA). A $400 \mu\text{m}$ -diameter nozzle is responsible for the impervious structure and a $200 \mu\text{m}$ diameter either “manufactures” or “is responsible for” the ML. A 1 mm-thick solid layer is added at the bottom of the FPM to guarantee that they are rigidly backed. The four FPMs are printed separately and then assembled with vacuum grease on their external walls. Images are shown in Fig. 2, illustrating the manufacturing of a FPM (a) and the assembled MpS (b) and (c). The supplementary material gives more information about the manufacturing process.

The skeleton of the porous medium, i.e., the ML, is rigid enough to be assumed motionless. The porous medium can, thus, be modeled as an equivalent fluid.¹ It accounts for viscous and thermal losses occurring inside the porous medium through its equivalent complex

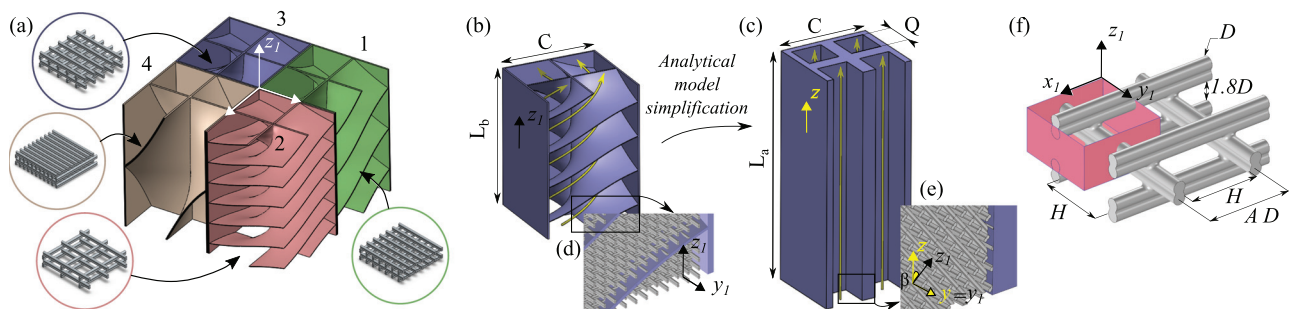


FIG. 1. Diagram of the MpS. (a) Schematic of parallel assembly of four FPMs of different ζ values filled by MLs of different IF values. (b) Single FPM, $\zeta = 1$, impervious structure. The gold arrows represent the circular helix of the mean acoustic path of length L_a . (c) Impervious structure of a FPM analytical model simplification. (d) FPM filled by the ML, detailed view. (e) FPM analytical model simplification, detailed view. (f) ML idealized micro-structure. The box delimits a unit cell.

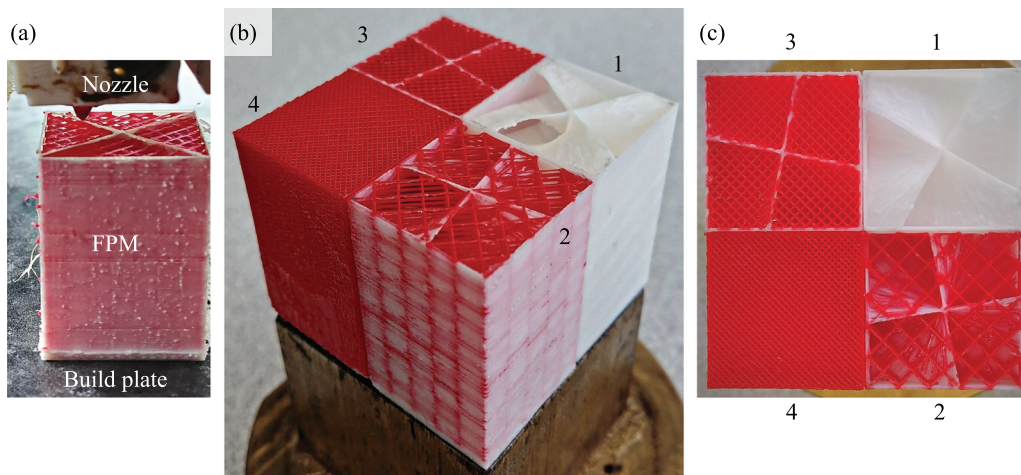


FIG. 2. Pictures of the optimized and 3D-printed MpS. (a) Single FPM being 3D printed. (b) Lateral and (c) top view of the MpS.

and frequency-dependent density ρ and bulk modulus K . An equivalent quasi-isotropic fluid implies that K is scalar, while ρ is a 3×3 diagonal matrix in the $(O, \mathbf{x}_1, \mathbf{y}_1, \mathbf{z}_1)$ frame, where $\rho_{x_1 x_1} = \rho_{y_1 y_1} \neq \rho_{z_1 z_1}$. According to the well-known Johnson–Champoux–Allard–Lafarge (JCAL) model,²⁵ the expression of the equivalent fluid properties can be approximated by means of six parameters related to the porous medium micro-structure in the case of isotropic media²⁵ and nine parameters in the case of the considered quasi-isotropic medium²⁶ (see the [supplementary material](#)).

The lattice constant, governed by the IF in practice, directly influences the ML micro-structure and consequently its equivalent fluid properties. In particular, reducing the lattice constant, i.e., stepping the IF up, increases the intrinsic losses of the ML. The JCAL parameter dependence on the IF of the ML was obtained by a two-scale asymptotic homogenization method^{27–29} combined with the inverse characterization³⁰ of a set of eight homogeneous samples followed by an interpolation over the IF range.⁶ The JCAL parameters of the characterized samples along with their interpolation ($IF \in [3; 60]\%$) are presented in the [supplementary material](#).

The MpS will be placed in a rigid backing configuration inside a square cross section waveguide and excited by a normal incidence plane wave. The walls of the waveguide act as mirrors for the pressure waves, and a periodic pattern of the MpS is then virtually created. Therefore, an infinite wall covered by a periodic distribution of the MpS will be evaluated. This configuration is first theoretically and numerically studied.

The analytical model does not account for the complex geometry of the FPMs. Instead, each FPM of height L_b and of cross sectional surface C^2 is approximated as a quadruplet of straight QWRs filled by porous media. They are of normal axis (O, \mathbf{z}) , of thickness $L_a(\xi) \geq L_b$ and of square cross section $Q^2(\xi) \leq C^2/4$ [see Fig. 1(c)]. For geometrical reasons and because the ML is quasi-isotropic, the principal direction \mathbf{z}_1 of the ML filling the QWRs forms an angle β with \mathbf{z} around $(O, \mathbf{y}) = (O, \mathbf{y}_1)$ [see Fig. 1(e) in the analytical model]. The latter uses a transfer matrix formulation adapted to anisotropic media³¹ for the propagation in the porous-filled QWRs and a modal

decomposition method considering Bloch modes in the surrounding air. Bloch waves account for the possible evanescent coupling between the different FPM in the MpS. From the numerical point of view, a full wave numerical simulation by FEM with the real geometry is used. Further information is given in the [supplementary material](#).

In both models, the MLs are represented by quasi-isotropic equivalent fluids defined by the JCAL model with the parameters obtained from inverse characterization. The walls of the structures are perfectly impervious and smooth, and their induced losses are not accounted for.³² Validation tests have shown that, on the one hand, the analytical model leads to very accurate predictions of the simplified geometry. On the other hand, the simplification of a FPM by a quadruplet of QWRs leads to slight shifts of the absorption coefficient in comparison to FEM predictions that grow with frequency.

The analytical model is used to optimize the geometry of an $L_b = 30$ mm-thick MpS to produce perfect absorption over a broadband frequency range. The optimization procedure, based on an iterative Nelder–Mead algorithm, aims to maximize the absorption coefficient in a targeted range of frequencies. To do so, the optimal folding of each FPM, governed by their ξ , and their associated ML, governed by their IF , are optimized. During the optimization, and for manufacturing reasons, IF is restricted to integer values comprised between 3% and 60%. ξ is restricted to two-digit values comprised between 0 and 2. To help the algorithm find the absolute minimum of the problem, the starting ξ values were chosen such that $L_a(\xi_i) \approx \lambda_i/5$, with λ_i being the wavelength in air corresponding to the targeted frequency of the FPM i . The absorption coefficient α is maximized over the frequency range of $f = [1150; 2000]$ Hz by maximizing a cost function $J = \sum_f \alpha(f)$. Fourteen frequencies are considered with a linear spacing. The high-frequency limit was chosen so that the highest frequencies of the bandwidth are managed by a $\xi = 0$ FPM. The low-frequency limit used in this work allows a good balance between the absorption plateau frequency width and the height of its ripples. The analytically optimized MpS has the following parameters: $[\{\xi_i, IF_i(\%)\}] = [\{1.67, 3\}, \{1.28, 10\}, \{0.72, 36\}, \{0, 36\}]$, $i = 1, 2, 3$, and 4. The corresponding JCAL parameters are presented

TABLE I. JCAL parameters of the numerically optimized MpS.

i	ξ	IF	ϕ	$\frac{\alpha_{\infty}^{\prime\prime}}{\alpha_{\infty}^{\prime}}$	$\frac{\Lambda^{\prime\prime}}{\Lambda^{\prime}}$ (μm)	Λ^{\prime} (μm)	$\frac{q_0^{\prime\prime}}{q_0^{\prime}}$ (10^{-9} m^2)	q_0^{\prime} (10^{-9} m^2)
1	1.67	3%	0.99	1.00	1000	3300	59.3	756
				1.04	2800		702	
2	1.28	10%	0.94	1.02	394	1200	20.1	95.2
				1.07	575		95.2	
3	0.72	24%	0.81	1.20	156	463	5.35	14.1
				1.13	256		9.6	
4	0	36%	0.71	1.35	100	225	2.20	5.5
				1.18	151		2.96	

in Table I. Experimentally, for $i = 1$, the optimization gave the value of $IF = 3\%$. However, this value is problematic as it corresponds to a lattice constant of $AD = 6.7 \text{ mm} \approx C/3$. Each folded cavity of this FPM should contain a single fiber per cross section. This ML is then not anymore a homogeneous porous material, and its induced losses are comparable to those of the impervious walls, neglected in the models. Then, this ML is omitted during the manufacturing, i.e., $\{1.67, 3\}$ is replaced by $\{1.67, 0\}$.

The absorption coefficient of the optimized material is presented in Fig. 3. The green continuous line corresponds to the analytical results, and the black continuous line shows the numerical predictions. The FEM predicts $\alpha(f) > 0.96 \forall f \in [1160; 2060] \text{ Hz}$, i.e., $5.6L_b < \lambda < 9.9L_b$ and $\bar{\alpha} = 0.98$. The four absorption maxima are equal to 0.99 or 1.00 corresponding to the critical coupling condition for each of the FPMs. The correlation between the analytical results and the numerical predictions is very good, with a slight absorption shift

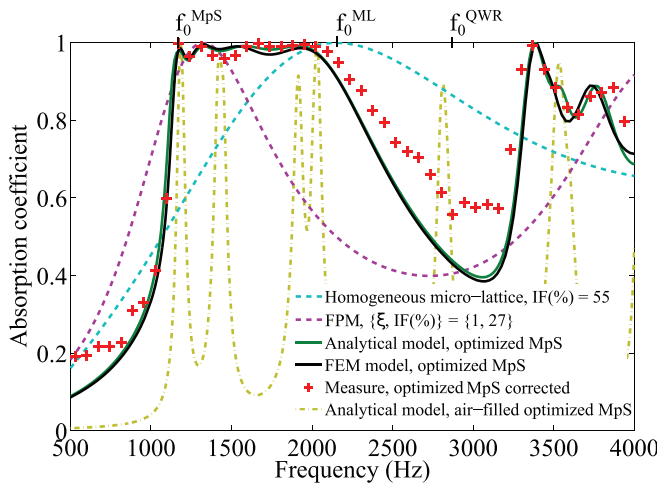


FIG. 3. Rigid-backing normal incidence absorption coefficient of $L_b = 30 \text{ mm}$ -thick materials. Critically coupled: homogeneous ML (blue dashed line) and $\xi = 1$ single FPM (purple dashed line). Simulation of the optimized MpS: analytical model (green solid line) and FEM model (black solid line). Measurement of the optimized MpS with adjusted IF (red crosses). Analytical simulation of the optimized MpS replacing the MLs by air (green dashed line). The f_0 marks highlight the frequency of the first absorption maximum of a 30 mm-thick QWR filled by air, the ML, and the MpS.

($\delta\alpha = 0.01$) between 1500 and 2000 Hz mainly due to the simplification of the geometry in the analytical model. The measurement (depicted in the supplementary material) is in agreement with the theoretical predictions, but the absorption is lower than expected between 1250 and 1700 Hz ($\delta\alpha = 0.07$). This frequency range corresponds to the absorption maxima of the second ($i = 2$) and third ($i = 3$) FPM. Perfect absorption occurs when the losses exactly compensate the leakages of the structure.¹² If the absorption is not perfect at the frequency of a maximum of absorption, it means that the associated losses are either too large or too small. Experimental investigations have shown that associated losses of the second and third FPM are too large experimentally, probably because the losses induced by the walls are neglected in the theoretical models. Then, another MpS was fabricated with reduced IF of such a FPM, i.e., with reduced inherent losses. The new MpS presents $IF_2(\%) = 7$ and $IF_3(\%) = 20$. This corresponds to a relative increase of 3% and 4% of the porosity, respectively. The absorption coefficient of this new MpS is depicted by the red crosses and $\alpha(f) > 0.96 \forall f \in [1155; 2140] \text{ Hz}$, i.e., $5.3L_b < \lambda < 9.9L_b$ and $\bar{\alpha} = 0.98$ are observed. The four absorption maxima are equal to 0.99 or 1.00 and are found logarithmically spaced in frequency as expected from Ref. 16 to achieve the mode density leading to a constant adapted impedance. The measured absorption is then in very good correlation with the theoretical predictions and slightly higher than that expected above 2140 Hz. The optimization procedure focused on maximizing the absorption in $f \in [1150; 2000] \text{ Hz}$. Above 2000 Hz, the absorption is not controlled and oscillates between low and high values. These high values are due to the harmonics of the FPMs. Conversely, the absorption deep between 2000 Hz and 3350 Hz comes from the absence of fundamental and of harmonic resonances in this frequency range. The absorption can be brought close to unity above 2000 Hz and until a very high frequency by increasing the number of resonators composing the MpS and tuning their resonances at frequencies for which the modal density is low in the presented configuration.¹⁶ Increasing the number of elements decreases the percentage of surface of the MpS covered by each element and decreases the absorption peak amplitude. This can be compensated by a porous layer added on top of the MpS flattening the absorption dips.^{16,33,34}

To highlight the crucial role of the MLs, that of the optimized MpS is replaced by air. The treatment is simulated analytically in the same way as the MpS, but Stinson's model³⁵ is used to account for the losses inside the cavities. The air-filled cavities are then simulated as four $L_a(\xi)$ height quadruplets of QWRs of hydraulic radius $Q(\xi)/\sqrt{\pi}$. The losses of such air-filled QWRs are not optimal, and they do not compensate the leakages. The losses are only induced by the folded geometry and, thus, by ξ . The analytically computed absorption coefficient of the air-filled folded material is depicted by the green dashed line in Fig. 3. The absorption maxima are sharp, and there is no absorption plateau close to unity. Moreover, it is worth noting here that a single FPM produces an absorption peak at longer wavelength than a homogeneous ML with the same L_b at the cost of a narrower absorption frequency width (Fig. 3, blue and purple dashed lines). However, the quality factor of the absorption peak of the FPM is much smaller than that of the QWR filled with air. This is the fundamental reason that explains the broadband character of the designed MpS in this work.

In this work, a folded metaporous material for sub-wavelength and broadband perfect absorption of sound is theoretically and

experimentally reported. The metaporous material consists of the assembly of several FPMs possessing sub-wavelength low-quality factor resonances. The geometry of each FPM is optimized in order to present perfect absorption at particular frequencies within a target frequency range. Therefore, the micro-lattice of the FPM is optimized to present the perfect balance between the inherent losses and the leakage of the resonator, giving rise to the critical coupling condition and as a consequence to the perfect absorption. An analytical model combining the modal decomposition and the transfer matrix method as well as a full wave numerical model are used to theoretically study the system. The analytical model is used to optimize the geometry for perfect absorption of sound at normal incidence for noise having a wavelength in air such that $5.6L_b < \lambda < 9.9L_b$. Relatively longer wavelengths could also be perfectly absorbed at the cost of narrower bandwidth. The structure is fabricated by 3D printing techniques, showing very good agreement with the theoretical results. Unlike folded liners, air-filled QWRs, or HRs, the losses of the introduced treatment are governed by a porous material. In this way, the losses of the treatment are independent of its impervious folded structure.

See the [supplementary material](#) of this Letter for further information about the equivalent fluid JCAL model and the variation of the JCAL parameters with respect to the IF , the manufacturing process, the numerical and analytical models including the geometry simplification of the FPM process, and, finally, the measurements.

The authors acknowledge Safran Aircraft Engines, the Natural Sciences and Engineering Research Council of Canada (NSERC) for supporting and funding this research. They acknowledge financial support from ANR industrial chair MACIA (No. ANR-16-CHIN-0002).

DATA AVAILABILITY

The data that support the findings of this study are available within this article and its [supplementary material](#).

REFERENCES

- J.-F. Allard and N. Atalla, *Propagation of Sound in Porous Media: Modelling Sound Absorbing Materials*, 2nd ed. (Wiley, Hoboken, NJ, 2009).
- L. Cao, Q. Fu, Y. Si, B. Ding, and J. Yu, "Porous materials for sound absorption," *Compos. Commun.* **10**, 25–35 (2018).
- T. G. Zielinski, "Pore-size effects in sound absorbing foams with periodic microstructure: Modelling and experimental verification using 3d printed specimens," in Proceedings of ISMA2016 International Conference on Noise and Vibration Engineering and USD2016 International Conference on Uncertainty in Structural Dynamics (2016).
- E. R. Fotsing, A. Dubourg, A. Ross, and J. Mardjono, "Acoustic properties of periodic micro-structures obtained by additive manufacturing," *Appl. Acoust.* **148**, 322–331 (2019).
- J. Boulvert, T. Cavalieri, J. Costa-Baptista, L. Schwan, V. Romero-García, G. Gabard, E. R. Fotsing, A. Ross, J. Mardjono, and J.-P. Groby, "Optimally graded porous material for broadband perfect absorption of sound," *J. Appl. Phys.* **126**, 175101 (2019).
- J. Boulvert, J. Costa-Baptista, T. Cavalieri, M. Perna, E. R. Fotsing, V. Romero-García, G. Gabard, A. Ross, J. Mardjono, and J.-P. Groby, "Acoustic modeling of micro-lattices obtained by additive manufacturing," *Appl. Acoust.* **164**, 107244 (2020).
- T. Parrott, M. Jones, and B. Homeijer, "Effect of resonator axis skew on normal incidence impedance," in *9th AIAA/CEAS Aeroacoustics Conference and Exhibit* (American Institute of Aeronautics and Astronautics, Hilton Head, SC, 2003).
- B. Howerton and T. Parrott, "Validation of an acoustic impedance prediction model for skewed resonators," in *15th AIAA/CEAS Aeroacoustics Conference (30th AIAA Aeroacoustics Conference)* (American Institute of Aeronautics and Astronautics, Miami, FL, 2009).
- X. Cai, Q. Guo, G. Hu, and J. Yang, "Ultrathin low-frequency sound absorbing panels based on coplanar spiral tubes or coplanar Helmholtz resonators," *Appl. Phys. Lett.* **105**, 121901 (2014).
- R. J. Beckemeyer and D. T. Sawdy, "Analytical and experimental studies of folded cavity duct acoustic liners," *J. Acoust. Soc. Am.* **60**, S123–S123 (1976).
- D. T. Sawdy and R. J. Beckemeyer, "Bandwidth attenuation with a folded cavity liner in a circular flow duct," *AIAA J.* **18**, 766–773 (1980).
- V. Romero-García, G. Theocharis, O. Richoux, and V. Pagneux, "Use of complex frequency plane to design broadband and sub-wavelength absorbers," *J. Acoust. Soc. Am.* **139**, 3395–3403 (2016).
- J.-P. Groby, R. Pommier, and Y. Aurégan, "Use of slow sound to design perfect and broadband passive sound absorbing materials," *J. Acoust. Soc. Am.* **139**, 1660–1671 (2016).
- Y. Li and B. M. Assouar, "Acoustic metasurface-based perfect absorber with deep subwavelength thickness," *Appl. Phys. Lett.* **108**, 063502 (2016).
- K. Donda, Y. Zhu, S.-W. Fan, L. Cao, Y. Li, and B. Assouar, "Extreme low-frequency ultrathin acoustic absorbing metasurface," *Appl. Phys. Lett.* **115**, 173506 (2019).
- M. Yang, S. Chen, C. Fu, and P. Sheng, "Optimal sound-absorbing structures," *Mater. Horiz.* **4**, 673–680 (2017).
- L. Lagarrigue, J.-P. Groby, V. Tournat, O. Dazel, and B. Nennig, "Acoustic panel," U.S. patent 20160210955A1 (August 2013).
- J.-P. Groby, A. Duclos, O. Dazel, L. Boeckx, and W. Lauriks, "Absorption of a rigid frame porous layer with periodic circular inclusions backed by a periodic grating," *J. Acoust. Soc. Am.* **129**, 3035–3046 (2011).
- C. Lagarrigue, J. P. Groby, V. Tournat, O. Dazel, and O. Umnova, "Absorption of sound by porous layers with embedded periodic arrays of resonant inclusions," *J. Acoust. Soc. Am.* **134**, 4670–4680 (2013).
- J.-P. Groby, C. Lagarrigue, B. Brouard, O. Dazel, V. Tournat, and B. Nennig, "Enhancing the absorption properties of acoustic porous plates by periodically embedding Helmholtz resonators," *J. Acoust. Soc. Am.* **137**, 273–280 (2015).
- Y. Zhou, D. Li, Y. Li, and T. Hao, "Perfect acoustic absorption by subwavelength metaporous composite," *Appl. Phys. Lett.* **115**, 093503 (2019).
- J.-P. Groby, W. Lauriks, and T. E. Vigran, "Total absorption peak by use of a rigid frame porous layer backed by a rigid multi-irregularities grating," *J. Acoust. Soc. Am.* **127**, 2865–2874 (2010).
- X. Zhu, K. Li, P. Zhang, J. Zhu, J. Zhang, C. Tian, and S. Liu, "Implementation of dispersion-free slow acoustic wave propagation and phase engineering with helical-structured metamaterials," *Nat. Commun.* **7**, 11731 (2016).
- M. Versaevael, L. Moreau, and E. Lacouture, "Folded spiral-shaped cavities for nacelle acoustic liners: Impedance and attenuation modelling and comparison to experimental results," in *3AF Greener Aviation 2016*, Bruxelles (2016), p. 9.
- D. Lafarge, P. Lemarinier, J. Allard, and V. Tarnow, "Dynamic compressibility of air in porous structures at audible frequencies," *J. Acoust. Soc. Am.* **102**, 1995–2006 (1997).
- V. Tarnow, "Compressibility of air in fibrous materials," *J. Acoust. Soc. Am.* **99**, 3010–3017 (1996).
- J.-L. Auriault, C. Boutin, and C. Geindreau, *Homogenization of Coupled Phenomena in Heterogeneous Media* (Wiley, 2009), oCLC: 733729827.
- C.-Y. Lee, M. J. Leamy, and J. H. Nadler, "Numerical calculation of effective density and compressibility tensors in periodic porous media: A multi-scale asymptotic method," in Proceedings of the COMSOL Conference (2008).
- A. Terroir, L. Schwan, T. Cavalieri, V. Romero-García, G. Gabard, and J.-P. Groby, "General method to retrieve all effective acoustic properties of fully-anisotropic fluid materials in three dimensional space," *J. Appl. Phys.* **125**, 025114 (2019).
- M. Niskanen, J.-P. Groby, A. Duclos, O. Dazel, J. C. Le Roux, N. Poulain, T. Huttunen, and T. Lahivaara, "Deterministic and statistical characterization of

- rigid frame porous materials from impedance tube measurements,” *J. Acoust. Soc. Am.* **142**, 2407–2418 (2017).
- ³¹T. Cavaliere, J. Boulvert, L. Schwan, G. Gabard, V. Romero-García, J.-P. Groby, M. Escouflaire, and J. Mardjono, “Acoustic wave propagation in effective graded fully anisotropic fluid layers,” *J. Acoust. Soc. Am.* **146**, 3400–3408 (2019).
- ³²W. Huang, L. Schwan, V. Romero-García, J.-M. Gènevaux, and J.-P. Groby, “3D-printed sound absorbing metafluid inspired by cereal straws,” *Sci. Rep.* **9**, 8496 (2019).
- ³³S. Huang, Z. Zhou, D. Li, T. Liu, X. Wang, J. Zhu, and Y. Li, “Compact broadband acoustic sink with coherently coupled weak resonances,” *Sci. Bull.* **65**, 373–379 (2020).
- ³⁴J.-P. Groby, B. Brouard, O. Dazel, B. Nennig, and L. Kelders, “Enhancing rigid frame porous layer absorption with three-dimensional periodic irregularities,” *J. Acoust. Soc. Am.* **133**, 821–831 (2013).
- ³⁵M. R. Stinson, “The propagation of plane sound waves in narrow and wide circular tubes, and generalization to uniform tubes of arbitrary cross-sectional shape,” *J. Acoust. Soc. Am.* **89**, 550–558 (1991).